Flow (2021), **This draft was prepared using the LaTeX style file belonging to FLOW: Applications of Fluid Mechanics** E1
doi:

RESEARCH ARTICLE

Effect of aspect ratio on the propulsive performance of tandem flapping foils

N. S. Lagopoulos [1,3*], G. D. Weymouth [2,4*], B. Ganapathisubramani [1]

[1] Aerodynamics and Flight Mechanics Group, University of Southampton, UK
[2] Southampton Marine and Maritime Institute, University of Southampton, UK
[3] Dolprop Industries AB, Ekerö, Sweden
[4] Alan Turing Institute, London, UK
*Corresponding authors. E-mails: nikolaos@dolprop.se and g.d.weymouth@soton.ac.uk

Received: XX 2021; **Revised:** XX XX 2021; **Accepted:** XX XX 2021

Keywords: Vortex dynamics; Swimming/flying; Autonomous underwater vehicles

Abstract

In this work, we describe the impact of aspect ratio (AR) on the performance of optimally phased, identical flapping flippers in a tandem configuration. Three-dimensional simulations are performed for seven sets of single and tandem finite foils at a moderate Reynolds number, with thrust producing, heave-to-pitch coupled kinematics. Increasing slenderness (or aspect ratio - AR) is found to improve thrust coefficients and thrust augmentation but the benefits level off towards higher values of AR. On the other hand, the propulsive efficiency shows no significant change with increasing AR, while the hind foil outperforms the single by a small margin. Further analysis of the spanwise development and propagation of vortical structures allows us to gain some insights into the mechanisms of these wake interactions and provide valuable information for the design of novel biomimetic propulsion systems.

Impact Statement Tandem flapping foils has the potential to be used for propulsion, especially among bio-inspired AUV designers, due to their superior performance over single flippers. In this study, we evaluate the importance of aspect ratio on the thrust-augmenting effect of in-line flapping, known as wake recapture. It is shown that flipper elongation impacts the interaction between the hind flipper (or follower) and its incoming flow, as it strengthens the vortices, shed in the wake of the front flipper. This affects both the thrust generating capacity and the optimal phasing of the flippers, allowing the engineer to determine the vehicle´s suitability towards certain missions, simply based on foil slenderness. An in-depth analysis of the wake dynamics enables us to distinguish the limitations as well as ways to optimize this approach by monitoring the transition towards a quasi two-dimensional flow.

1. Introduction

Flapping foil mechanisms are the basic means of propulsion and control within the avian and aquatic fauna. These systems are often more agile, durable and efficient compared to conventional man-made propulsors (Weymouth, 2016). Thus, many studies have focused on the analysis of these biological configurations in terms of kinematics (Khalid et al., 2021; Cimarelli et al., 2021) fluid-structure interaction (Kim et al., 2013; Zurman-Nasution et al., 2020) as well as the effects of planform geometry (Dagenais and Aegerter, 2020; Zurman-Nasution et al., 2021b) and flexibility (Shi et al., 2020; Fernandez-Feria and Alaminos-Quesada, 2021).

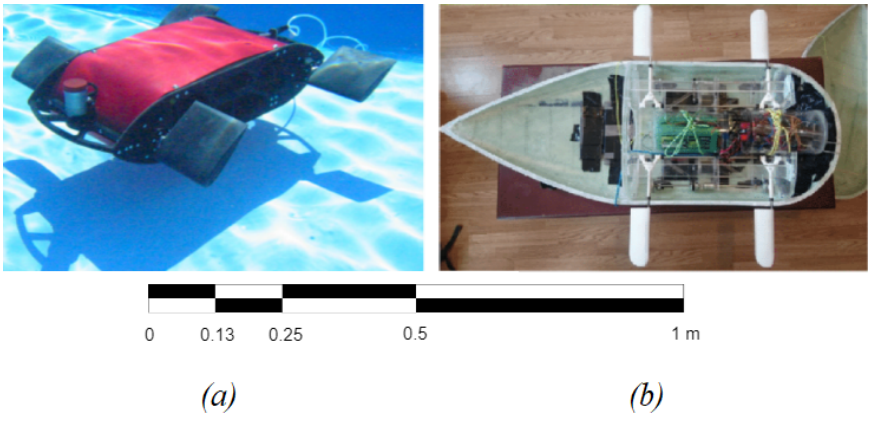

Figure 1. *Two examples of bio-inspired AUVs that combine front and back flipper oscillation (tandem arrangement) as a means of propulsion: (a) performs a pure pitching motion (Long et al., 2006) while (b) uses a combination of rolling and pitching (Weymouth et al., 2017). A simplified version of the latter kinematics is utilized by this study.*

Tandem flapping configurations e.g. insect wings (Alexander, 1984; Thomas et al., 2004), plesiosaur flippers (Robinson and JA, 1975; Hawthorne et al., 2019) etc. are shown to outperform single flappers due to certain foil-wake interactions commonly referred to as *wake recapture* (Broering and Lian, 2012; Muscutt et al., 2017b). This has inspired researchers to experiment on quadruple foil systems to propel autonomous underwater vehicles (AUVs), utilizing a variety of harmonic kinematics e.g pitch, roll, coupled motion etc. Most of these tetrapodal swimmers (see figure 1) are electric-powered, designed for a wide range of depths ($1m - 100m$) and can reach velocities of $0.5m/s - 2m/s$ (Licht et al., 2004; Long et al., 2006; Weymouth et al., 2017), which are comparable to modern propeller-driven, ocean-going AUVs of a similar size and weight (Yuh, 2000).

Of particular interest, towards the design of these systems, is the *aspect ratio* AR (for rectangular wings AR = W/C where W is the wingspan and C is the chord length) due to its impact on the system´s thrust generation capacity. Slender flippers for example, are widely considered beneficial to both thrust and efficiency (Green and Smits, 2008; Shao et al., 2010; Dewey et al., 2013) which is further implied by the predominance of high AR wings among birds and insects (Ellington, 1984; Azuma, 1992; Usherwood and Ellington, 2002). As a result, early research was driven towards two dimensional or quasi two dimensional approaches both experimentally (Koochesfahani, 1989; Triantafyllou et al., 1993) and numerically (Pedro et al., 2003; Mittal, 2004; Guglielmini and Blondeaux, 2004).

Unlike avian organisms however, aquatic animals demonstrate a great variety of AR with non migratory fish utilizing mostly low AR (Walker and Westneat, 2002; Combes and Daniel, 2001) as they are considered more suitable for their drag-based paddling motion. Furthermore, comparisons among various species suggest that high AR‘s benefit cruising efficiency while low AR‘s promotes thrust generation in short bursts (Flammang and Lauder, 2009; Domenici, 2010) which is also supported by recent experiments (Lee et al., 2017). A preference towards lower AR in aquatic propulsion can be additionally attributed to the much higher density of water, which leads to greater added-mass associated bending moments (Dong et al., 2006). This can significantly constrain the design of an AUV by determining manufacturing costs, durability, mission envelope etc. and thus demonstrates the necessity of finite flipper analysis.

Contemporary literature on finite wings of varying AR often focuses on single flapping configurations (Zurman-Nasution et al., 2021b; Hammer et al., 2021; Zhong et al., 2021) with only a few studies related to tandem arrangements (Arranz et al., 2020; Jurado et al., 2022). A key feature of the above is the presence of tip vortices that transform the two dimensional wake into a complex chain of ring-like formations (Shao et al., 2010; Li et al., 2018). Moreover, the majority of these studies utilizes insect and

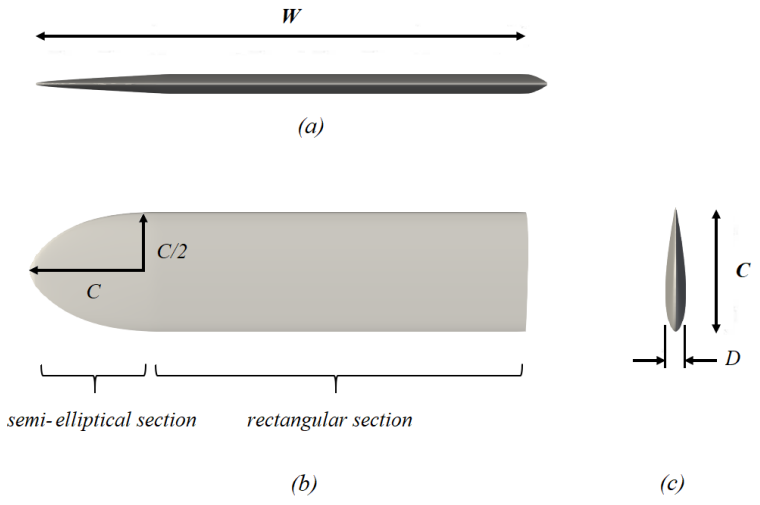

Figure 2. *Structural details of an AR=4 hydrofoil, where the (a) frontal,(b) upper and (c) side view are presented. A detailed model of the flipper in the form of an IGS file can be found online, within the supplementary material of this study.*

small fish kinematics and/or geometries which, although quite suitable for special applications, are less relevant to open water designs. On the other hand, certain heave-to-pitch combinations are considered dominant in cetacean locomotion (Ayancik et al., 2020; Han et al., 2020) (where spanwise flexibility of the caudal fin is comparatively low (Gough et al., 2018; Adams and Fish, 2019)). Furthermore, heave-to-pitch coupling is considered sufficient to represent the mid-chord kinematics of flipper-based, AUV´s and/or aquatic animals using roll-to-pitch combinations (Muscutt et al., 2017a) such as sea turtles, penguins and most notably the tetrapodal plesiosaurs (Carpenter et al., 2010). Besides, the effect of flipper AR on the wake recapture remains unknown, despite its aforementioned importance within tandem flapping AUV consepts.

The present study attempts to address these issues via the numerical analysis of rectangular flippers with elliptical tip, undergoing heave-to-pitch coupling for a chord based Reynolds number, $Re_C = \rho U_\infty C/\mu = 8500$ where ρ is the water density, U_∞ is the freestream velocity and μ is the dynamic viscosity. Seven AR are tested in both single and tandem configurations of identical AR for an amplitude based Strouhal, $St_A = f \cdot 2\mathcal{A}/U_\infty = 0.4$ where f is the frequency of oscillation and $2\mathcal{A}$ is the peak-to-peak amplitude of the trailing edge (TE) (Triantafyllou et al., 1991). In addition, the phase lag and distance between consecutive flippers are kept constant, selected for maximum thrust augmentation at the given St_A in 2D (Muscutt et al., 2017b). Here, the choice of St_A is based on the observed range of Strouhals utilized by swimming and flying organisms (Triantafyllou et al., 1993). Furthermore, the test cases are evaluated in terms of load coefficients, relative thrust augmentation and hydrodynamic efficiency. To this end, we compare the single/tandem flipper sensitivity to AR and attempt to shed light on the three dimensional aspect of the wake to wake interaction.

2. Methodology

2.1. Flipper geometry and kinematics

We consider a rigid NACA0016 with a thickness $D = 0.16\,C$, a rectangular planform section where the width is equal to 1 C and a tapered elliptical tip as shown in figure 2. Here the elliptical section has a span of 1 C while W is the total span of the flipper. Thus, for the sake of simplicity, we use the AR

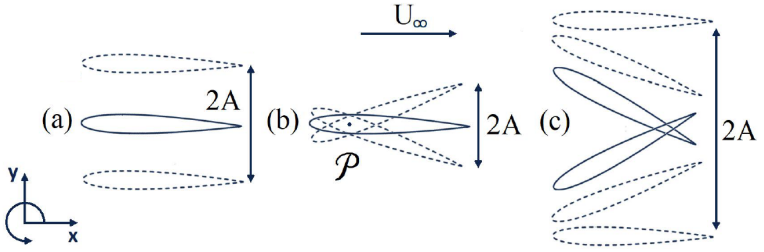

Figure 3. *The kinematic parameters and coordinate system of an oscillating foil undergoing (a) heave (b) pitch and (c) coupled motion. Redrawn from (Lagopoulos et al., 2019).*

definition of rectangular flippers (explained in section 1) and we set our baseline test case at AR = 2 proceeding towards AR = 8 in increments of AR = 1.

The kinematics parameters of the hydrofoil can be seen in figure 3. As stated above, the flippers utilize heave to pitch coupling which is achieved by the superposition of the two harmonic components. More specifically, pitch refers to the sinusoidal rotation about the pivot point $\mathcal{P} = 0.25$ (normalised by C) while heave is a sinusoidal, vertical translation with respect to the centreline. Thus the combined motion of the TE can be described as:

$$y_f(t) = \underbrace{h_0 \sin(2f\pi t)}_{y_h(t)} + \underbrace{(1-\mathcal{P})C \sin[\theta(t)]}_{y_\theta(t)} \tag{1}$$

$$with \quad \theta(t) = -\theta_0 \sin(2f\pi t + \psi) \tag{2}$$

where subscripts f, h and θ denote the front (or single foil), heaving and pitching components respectively.

Here, the instantaneous pitching angle is expressed as the $\theta(t)$, while h_0 and θ_0 represent the amplitudes of the two motions. Note that although the total peak-to-peak amplitude is a combination of these TE displacements, the chosen kinematic parameters result in $\mathcal{A} \sim h_0 = 1\,C$. Furthermore, the heave to pitch phase difference is set to $\psi = 90°$, which is shown to maximize the propulsive efficiency within the frequency range of interest (Platzer and Jones, 2008). Lastly, the combined (or effective) angle of attack $\alpha(t)$ equals to the summation of $\theta(t)$ and the heave-induced angle of attack. For the current range of kinematic parameters (i.e., amplitudes and frequencies) the amplitude of the effective angle of attack can be approximated as:

$$\alpha_0 = \arctan\frac{2\pi f h_0}{U_\infty} - \theta_0 \tag{3}$$

where $2\pi f h_0$ is the amplitude of dy_h/dt. Within this study, all simulations are conducted for $\alpha_0 = 20°$ due to its dominance within modern cetaceans (Fish and Rohr, 1999) and relevant studies in tetrapodal swimming (Muscutt et al., 2017a).

The complete tandem arrangement is depicted in figure 4. To distinguish parameters referring to the front or the back foil, we utilize the subscripts f (already mentioned above) and b respectively, for the remaining of this study. Furthermore, to describe the foil-to-foil interaction, we introduce two more parameters: the *phase lag* and the inter foil *spacing*.

The phase lag between the two foils is expressed as ϕ and will be referred to as simply the $phase$. Thus the back flipper´s motion is described as:

$$y_b(t) = y_h(t+\phi) + y_\theta(t+\phi) \tag{4}$$

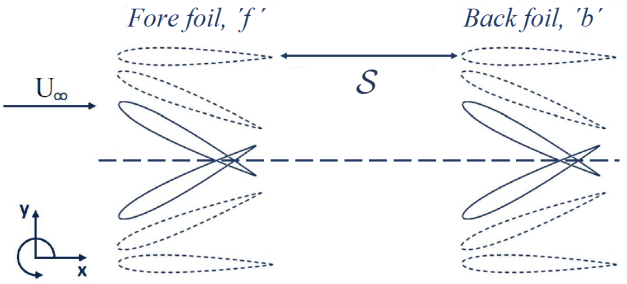

Figure 4. *Details of a tandem foil configuration, undergoing synchronous ($\phi = 0°$), heave-to-pitch coupling.*

Here, $\phi = 0^o$ as preliminary simulations found that this increases the overall thrust of the hind foil for the chosen parameters (for details see Appendix A).

Spacing $\mathcal{S}$ is the distance between the TE of the front foil and the leading edge (LE) of the back foil towards the streamwise direction. Therefore the chord normalised spacing $\mathcal{S}_C$ is defined as:

$$\mathcal{S}_C = \frac{\mathcal{S}}{C} \tag{5}$$

While a $\mathcal{S}_C \leq 1$ is dominant among small fliers such as dragonflies (Broering and Lian, 2012; Usherwood and Lehmann, 2008), fossils records suggest that $\mathcal{S}_C \geq 3$ was more common in plesiosaurs (Muscutt et al., 2017a; O'Keefe and Carrano, 2005). In our study $\mathcal{S}_C = 2$, which allows a relatively compact design and has demonstrated maximum thrust augmentation in tandem arrangements of similar kinematics and St_A (Muscutt et al., 2017b).

2.2. Performance metrics

Within a flapping cycle, the flipper experiences the time-dependent thrust $F_X(t)$, the side (lateral) force $F_Y(t)$ and moment $M_Z(t)$ around $\mathcal{P}$. In this study we focus on the thrust generation capacity and lateral force development of the fore and hind flipper, characterised by the thrust and side force coefficients respectively:

$$C_T = \frac{F_X}{\frac{1}{2}\rho U_\infty^2 G} \quad , \quad C_Y = \frac{F_Y}{\frac{1}{2}\rho U_\infty^2 G} \tag{6}$$

where $G = C \cdot (W - C) + 0.25\pi C^2$ is the planform area. Cycle averaged quantities are presented with a tilde ($\widetilde{\ }$) to distinguish them from their instantaneous counterparts. Furthermore, the two dimensional thrust coefficient (where G is replaced by C) is distinguished by the use of the subscript t instead of T.

Another important parameter is the propulsive (hydrodynamic) efficiency (η) of each flipper. This is simply the ratio between the power of the generated thrust and the power imparted to the flipper so that it overcomes the loads imposed by the fluid:

$$\eta = \frac{TU_\infty}{P} \tag{7}$$

where T is the thrust and P the input power defined as:

$$P(t) = F_Y(t)\frac{dy_h(t)}{dt} + M_Z(t)\frac{d\theta(t)}{dt} \tag{8}$$

To compare the performance of the single and tandem configurations we normalize the above values by the equivalent parameters of the single (front) flipper:

$$C^*_{T,b} = \frac{\tilde{C_{T,b}}}{\tilde{C_{T,f}}} \quad , \quad \eta^*_b = \frac{\eta_b}{\eta_f} \tag{9}$$

where * denotes relative terms. Previous studies suggest little to no alteration of the front foil´s loads and efficiency by the presence of the hind for $S_C \geq 1$ (Muscutt et al., 2017b). Thus, any normalised parameters presented here are associated with the back flipper.

2.3. Computational method

The numerical package used for this work is based on the boundary data immersion method (BDIM). BDIM is able to simulate the entire domain by combining the full Navier-Stokes equations and the prescribed solid kinematics through a kernel function (Weymouth and Yue, 2011). Here, the equations are solved on a Cartesian finite volume grid, where the convective term is expressed by a flux-limited Quadratic Upstream Interpolation for Convective Kinematics (QUICK) scheme (Leonard, 1979) and the diffusive terms are handled via central differences. Temporal discretization is achieved via Heun's explicit second-order method and an adaptive time-stepping scheme is utilized to preserve stability (Polet et al., 2015). Moreover, turbulence is described through an implicit Large Eddy Simulation (iLES) model that utilizes flux limiting to model the energy dissipation caused by sub-grid stress (Lauber et al., 2022). iLES modelling is well suited to intermediate Reynolds numbers such as those utilized in the present study, and Hendrickson et al. (2019) demonstrates that this iLES model completely deactivates when the grid is sufficiently fine to resolve the physical dissipation. In addition, BDIM has been validated for flapping foil applications at a wide range of kinematics and Reynolds numbers of up to 10^5, resulting in thrust prediction errors of $\epsilon \leq 5\%$ (Maertens and Weymouth, 2015).

The 2D computational domain is formed by a rectangular mesh with a dense uniform zone around the body and near wake, while exponential grid stretching is used for the far-field. In particular, the inlet is located $2C$ ($0.5C$ for the uniform zone) ahead of the front foil´s $\mathcal{P}$ and the outlet is placed at $14C$ ($9C$ for the uniform zone) downstream. Moreover, regarding the upper/lower boundaries, the foils are placed in the middle, keeping a distance of $6C$ ($2C$ for the uniform zone) from both sides. Finally, to avoid discrepancies between 2D and 3D results, the 3D mesh configurations are derived from the 2D by simply extending the domain towards the spanwise direction (z axis). Here, the uniform grid exceeds the flipper span by $0.2C$ to include possible wingtip effects (Zurman-Nasution et al., 2021a) while the non-uniform increases proportionally with AR, allowing a flipper-to-boundary distance = $1.25W$ for all text cases (e.g. at $AR = 2$ the spanwise domain is $4.5C$ long, while at $AR = 8$ it reaches $18C$).

In all the above cases, boundary conditions consist of a uniform inflow, zero-gradient outflow and free-slip conditions on the upper and lower boundaries. Moreover, no-slip conditions are imposed on the oscillating foil and, for the 3D simulations, symmetric conditions are enforced towards the two spanwise directions.

A convergence analysis is conducted with the mesh density being expressed in terms of grid points per chord. More specifically, in the case of the uniform zone, a grid of $\Delta x = \Delta y = \Delta z = C/64$ is used, yielding relatively fast results while the standard deviation of the estimated thrust is $\leq 8\%$ of the simulations with four times the resolution in both 2D and 3D (Zurman-Nasution et al., 2021a).

3. Results and discussion

3.1. AR effect on the single flipper

The performance of the single flipper at varying AR can be seen in figure 5. Elongation leads to a sharp increase of the thrust coefficient until $AR \sim 4$ where the curve starts to asymtote for higher AR

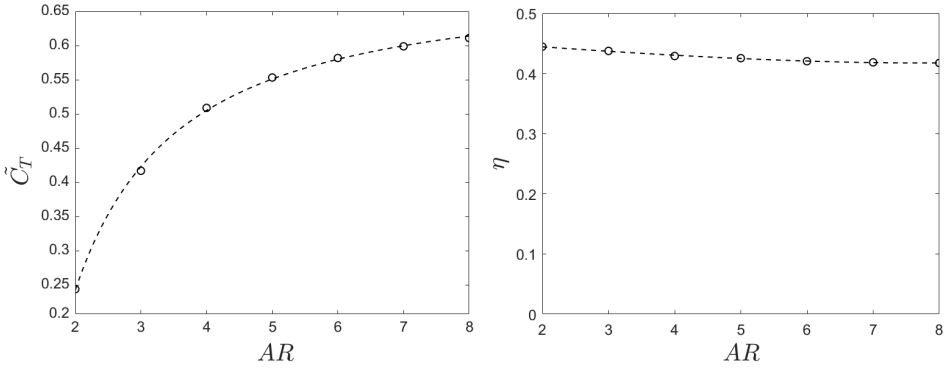

Figure 5. *The impact of AR on the (a) thrust coefficient and (b) efficiency of the single flipper, undergoing heave-to-pitch coupling. Simulation points are characterised by ∘ while the best fit curve is depicted via a dashed line.*

and $\frac{\delta \tilde{C_T}}{\delta AR} \leq 3\%$ (beyond AR > 6). However, a noticeable discrepancy still exists between the longest spans tested and the two dimensional case, where $\tilde{C_{t,f}} = 0.675$ (see Appendix A). Unlike $\tilde{C_T}$, the propulsive efficiency seems almost insensitive to slenderness, possibly due to the use of an optimal St_A (Triantafyllou et al., 1993; Dong et al., 2006), with a negligible decline observed for AR between 2 and 4.

A qualitative comparison of the flow field around different AR´s can be seen in figure 6, where the wake is visualized during the mid-upstroke, via the Q-criterion (King et al., 2018). Animations of the vorticity fields for the single, $AR = 2$ and $AR = 8$ test cases can be found in the on-line supplementary movies and are entitled singleAR2 and singleAR8 respectively. Due to the combined heave and pitch, all cases experience shallow, dynamic separations (Ol et al., 2010) throughout the flapping cycle . In other words, an initially small leading edge vortex (LEV) travels backwards while remaining attached to the foil and eventually sheds near the TE at full size (Karbasian and Esfahani, 2017). Since the flow is three dimensional, this shed vortex resembles a cylindrical tube, which appears almost undisturbed by the tip effects (red box in figure 6d). Turbulent structures can be seen only downstream of the elliptical end, indicating local breakdown. This breakdown propagates towards the root covering a distance of 2.5 C which remains constant, regardless of the flipper AR (figures 6 a-c). Consequently, an increasing AR allows the formation of elongated, undisturbed vortices leading to quasi-two-dimensional wake.

In order to quantify the above observations, we examine changes in the strength of the downstream wake, for varying levels of planform slenderness. This can be achieved by calculating the circulation (Γ) of a LEV at a chosen instant of the flapping cycle, from a spanwise-averaged flow field. Variations along the span will be absorbed in this spanwise-averaging process leading to increased circulation for only the most coherent LEVs. Details of the procedure can be found in Appendix B. As shown in figure 7a, the LEV appears to become more compact for higher AR, causing Γ to saturate at a constant value (see figure 7b). This in turn, leads to a constant velocity surplus across the flipper span which is reflected in the similar behaviour of $\tilde{C_{T,f}}$ in figure 5.

Fundamentally, the development and propagation of the LEV is associated with the generation of circulatory (lift-based) forces (Karbasian and Esfahani, 2017; Muscutt et al., 2017b). Therefore, similarities in the convergence of $\tilde{C_{T,f}}$ and Γ towards high AR, imply that the main contributors of thrust under the chosen kinematics are lift-based. Indeed, heave-dominant motions have been mostly connected to circulatory forces while pitch-based kinematics are more affected by the added mass effect (Floryan et al., 2017; Van Buren et al., 2019). The latter has been linked to the peaked lateral forces in oscillating fins of similar geometry, undergoing rolling or twisting, at medium Re_C (Zurman-Nasution et al., 2021a). Motivated by these findings we plot the front foil's $C_{Y,max}$ for varying AR in figure 8b. Once again, a sharp force increase is observed for $AR \leq 4$ followed by a slow converge towards high

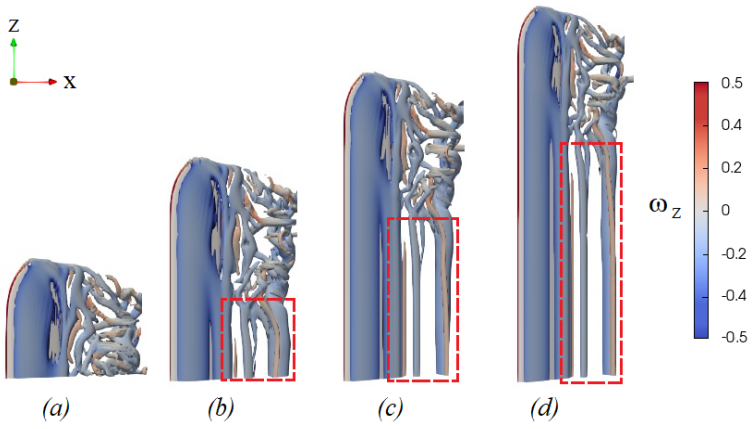

Figure 6. *Snapshots of normalised vorticity at $t/T = 1$ where $T = 1/f$, for single flappers of (a) $AR = 2$, (b) $AR = 4$, (c) $AR = 6$ and (d) $AR = 8$. Wake structures are visualized using iso-surfaces with 0.14% of Q_{max}. The direction of the free-stream flow U_∞ is right to left. Areas of undisturbed, two dimensional wake are characterised by rectangles of red dashed lines.*

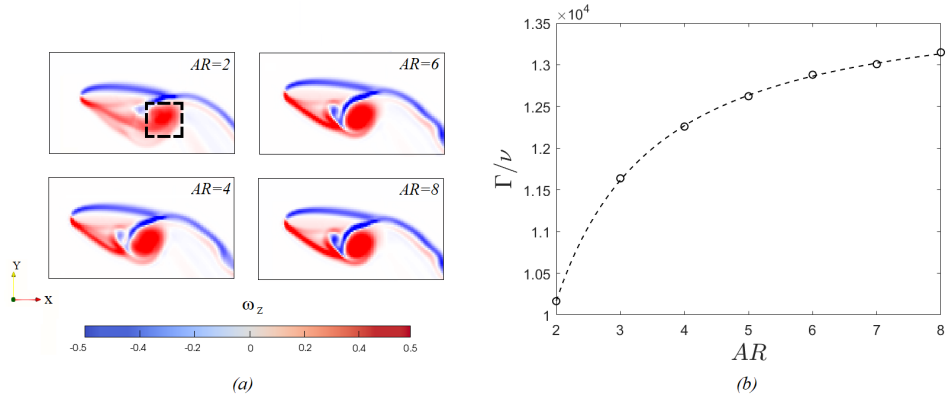

Figure 7. *(a) Spanwise averaged vorticity for single flippers at $t/T = 0.25$ where the LEV is enclosed by a box of black dashed line for $AR = 2$. (b) The resultant circulation over kinematic viscosity (ν) of the LEV, calculated at this instance for all AR´s of this study.*

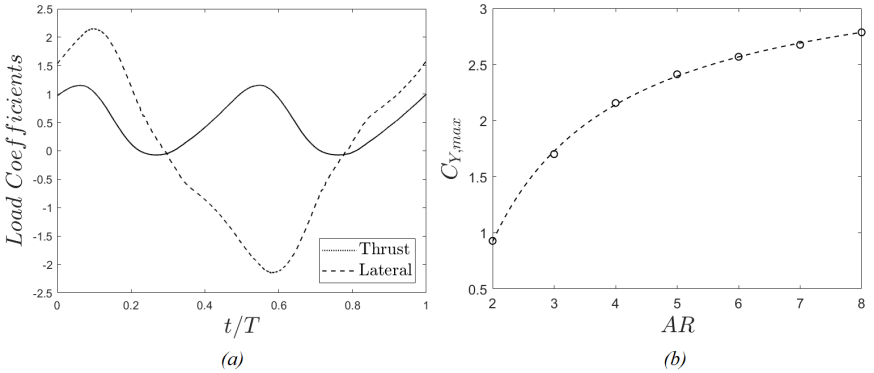

Figure 8. *(a) Temporal evolution of C_T and C_Y for the front flipper at $AR = 8$. (b) Development of the peak lateral force coefficient for the front flipper at varying AR. Simulation points are depicted as ○ while the dashed lines represent the best fit curves.*

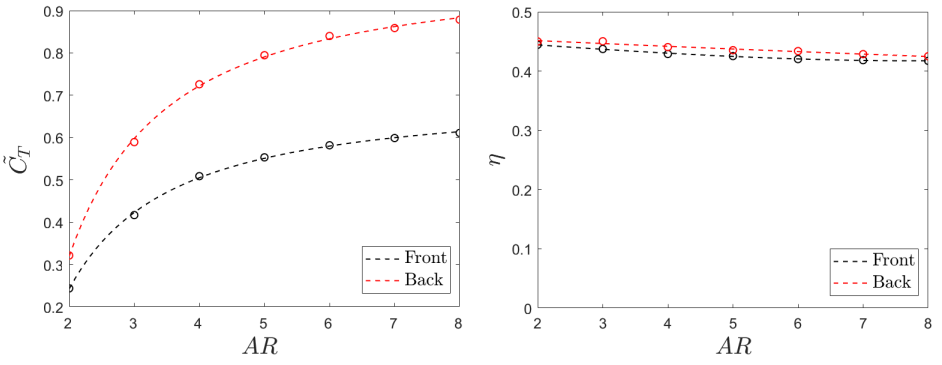

Figure 9. *The impact of AR in terms of (a) thrust coefficient and (b) efficiency, on the fore and hind flippers of a tandem configuration, undergoing heave-to-pitch coupling at $\phi = 0°$ and $\mathcal{S}_C = 2$. Simulation points are characterised by $\circ$ while the best fit curve is depicted via a dashed line.*

levels of slenderness. Consequently, we can argue that both the added mass and circulatory components experience a saturating effect towards high AR, while a more detailed separation of the two forces serves as a motivation for our future research.

Here, it is noteworthy to mention that similar $\tilde{C_T} - AR$ relationships to those shown previously, have been reported by Shao et al. (2010) despite the latter´s different planform geometry (no wingtip) and significantly lower Re_C. As both studies utilize heave-to-pitch coupling at $\psi = 90^o$, a similar dynamic separation should be expected at least in 2D. Moreover, the chosen kinematics are essentially two dimensional ($\frac{\delta y_f}{\delta z} = \frac{\delta y_b}{\delta z} = 0$), further reducing the importance of the spanwise geometry, although they still cause minor discrepancies between the two studies e.g. in $\tilde{C_T}$. This, in turn, can support the predominance of medium slenderness ($AR \sim [4, 6]$ using our paper´s definition) caudal fins observed in cetaceans (Woodward et al., 2006; Ayancik et al., 2020) where the same kinematics are used. Indeed, fins of too low AR would reduce the propulsive capacity of the species, yet much larger ones would be structurally demanding without offering any significant hydrodynamic advantage. It should be noted, however, that these animals demonstrate a plethora of wingtip geometries, combined with at least some level of flexibility (Fish and Rohr, 1999). Thus, although a deeper analysis in the area is required, this topic is beyond the focus of the present work.

3.2. AR effect on the tandem configuration

The addition of another upstream oscillating body alters the flow field and determines the performance of the downstream foil. This is made clear in figure 9a where the rear flipper demonstrates significantly higher $\tilde{C_T}$ than the front, due to wake recapture. Once again, elongation has a greater impact on low AR´s but $\tilde{C_T}$ appears to stabilize at a rate that is marginally slower than that of a single foil (or that of the front foil). This delayed convergence allows tandem systems to further improve their propulsive characteristics by reaching higher AR´s than the single test cases. On the other hand, the efficiency shows a negligible improvement while following the same trend as for the front foil (see figure 9b).

In order to investigate the relative augmentation of thrust for the back foil in more detail, we examine $\tilde{C_{T,b}}^*$ (from eq. 9) in figure 10a. It can be seen that there is a sharp increase in this ratio for $AR \sim [2, 4]$ (from $\tilde{C_{T,b}}^* = 1.3$ to $\tilde{C_{T,b}}^* = 1.45$) and the ratio seems to level out around AR = 4 (at $\tilde{C_{T,b}}^* \sim 1.42$) which remains approximately constant beyond this aspect ratio. This shows that the rate of increase in thrust for the front and back foils essentially follow each other proportionately. Thus, there are no further

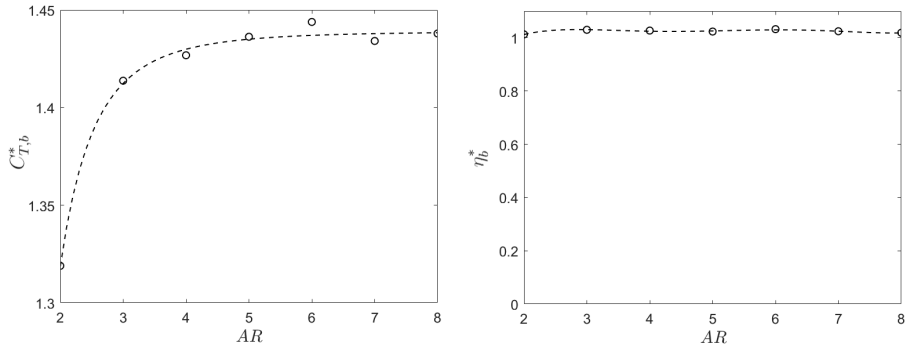

Figure 10. *The impact of AR, in terms of relative (a) thrust and (b) efficiency augmentation, on the hind flipper of the tandem configuration, undergoing heave-to-pitch coupling at $\phi = 0°$ and $\mathcal{S}_C = 2$. Simulation points are depicted as ∘ while the dashed lines represent the best fit curves.*

benefits beyond AR = 4 in terms of relative augmentation, although there is still a benefit in the overall thrust produced by the pair of flippers.

Interestingly, figure 10b shows that relative efficiency $\eta_b{}^*$ (which is the ratio of efficiency of back foil to the front foil) remains practically unchanged, showing minor growth of about 2.4% throughout the entire range of AR (see figure 10b). This has been reported in recent studies of in-line foils (Broering and Lian, 2015; Arranz et al., 2020) for a range of harmonic motions and can be linked to the St_A being already optimized for maximum efficiency on both flippers (similarly to the single foil cases). Yet, for a tandem setup the choice of a particular ϕ should be also taken into account. Indeed, flipper phasing has been shown to impact the hind foil´s efficiency in various tandem foil concepts (Broering and Lian, 2015; Xu et al., 2017; Muscutt et al., 2017b; Epps et al., 2017; Arranz et al., 2020). Therefore, proper alignment of the aforementioned parameters might result in further gains within this area. However, this is beyond the scope of our current study.

The above observations can be linked to the flow field development between the two foils. This is evident in figure 11, where the wakes of tandem arrangements for $AR = 2$ and $AR = 8$ are compared (animations of these test cases can be found in the supplementary material). As mentioned previously, wingtip effects are proportionally higher in the wake of $AR = 2$ compared to $AR = 8$ (figures 11a and 11b) resulting in the break-up of the foils' shed vortices (figures 11c and 11d). Specifically, the break-up of the LEV shed from the front foil means that the back foil does not experience a coherent wake across its span, which limits the benefits derived from wake recapture. Therefore, although a $\sim 30\%$ increase in thrust can be noteworthy (figure 10a for $AR = 2$), it is still far away from the optimal cases reported here or found in literature (Akhtar et al., 2007; Boschitsch et al., 2014; Xu et al., 2017; Muscutt et al., 2017b,a; Lagopoulos et al., 2020; Joshi and Mysa, 2021). It should be also noted that a similar, performance deterioration of in-line flapping due to 3D associated effects has been also witnessed within insect-like concepts, where lower Re_C and $\mathcal{S}_C$ have been utilized (Arranz et al., 2020). On the other hand, the propulsive enhancement derived from flipper elongation is not limitless. As the AR increases past a certain degree (here $AR \geq 4$), the incoming wake takes a quasi-2D form (except at around the tip) and the gains in $\tilde{C_{T,b}}{}^*$ begin to stagnate since no additional benefit can be extracted.

These findings can be further quantified by computing the spanwise-averaged circulation of the LEV for the back flipper at different aspect ratios. As shown in figure 12a, wake recapture allows the formation of a noticeably larger and stronger LEV compared with those shed by the front foil. However, its compactness/coherence is more dependent on flipper elongation, which alters the LEV circulation with AR (see figure 12b). Note that the circulation is computed based on a given box size and further information on the effect of box size on the computation of this circulation is in Appendix B. For low

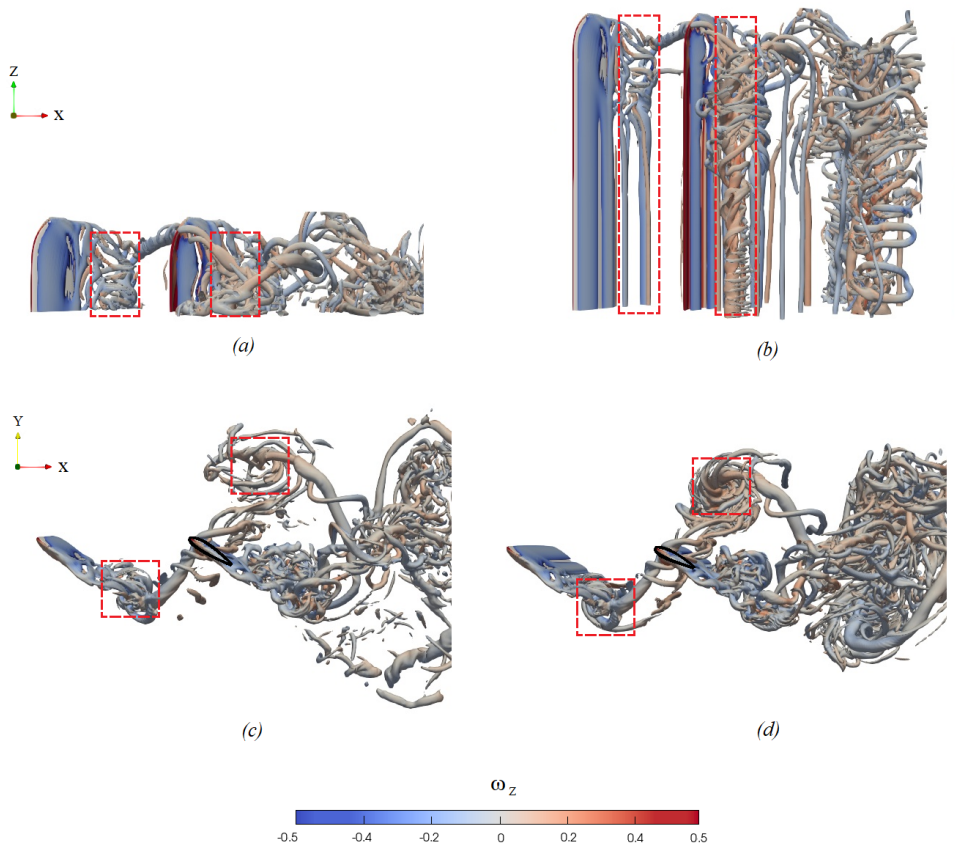

Figure 11. *Snapshots of normalised vorticity at $t/T = 1$ for tandem configurations, where the flow structures are visualized by using iso-surfaces with 0.14% of Q_{max}. A top view comparison shows that the wake of $AR = 2$ (a) suffers significantly from vortex breakdown while the wake of $AR = 8$ (c) remains mostly unaffected. This is more evident at a side view of $AR = 2$ (c) and $AR = 8$ (d), although the aft foil (highlighted with a black border) manages to weave through the incoming vortex pair (boxes of red dashed line) of the front flipper, due to proper ϕ adjustment.*

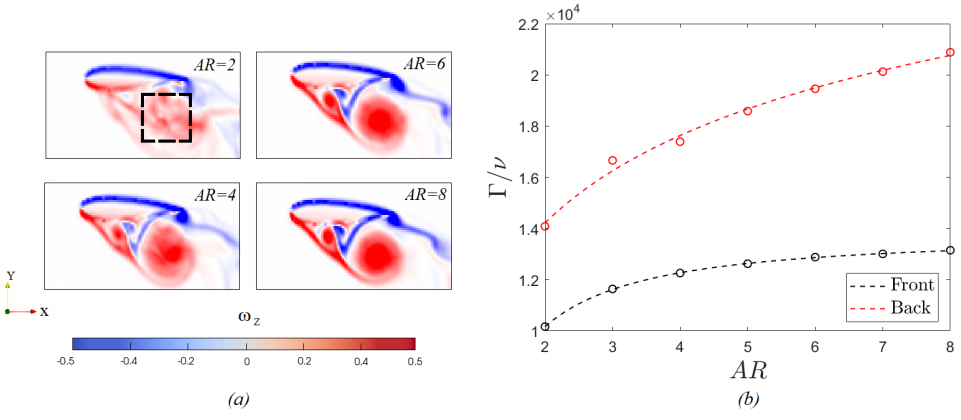

Figure 12. *(a) Spanwise averaged vorticity for back flippers of a tandem configuration, at $t/T = 0.25$ where the LEV is enclosed in a box of black dashed line for $AR = 2$. (b) The resultant Γ/ν calculated at this instance, for the LEV of both front and back foils with $AR \sim [2, 8]$.*

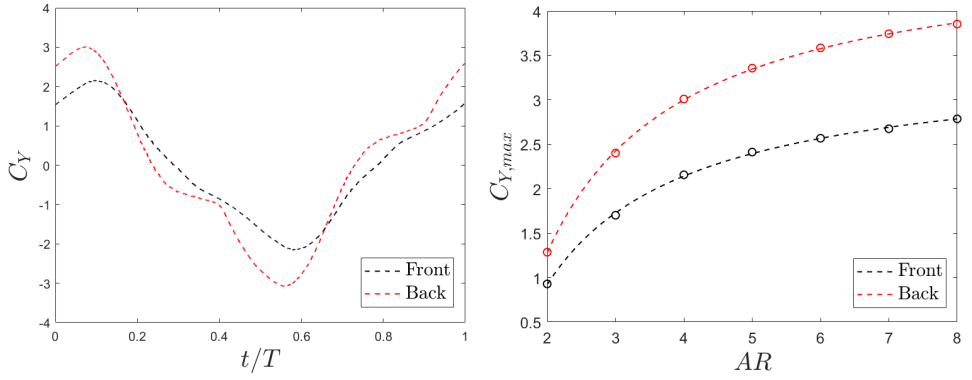

Figure 13. *(a) Temporal evolution of C_Y for both flippers at $AR = 8$. (b) Comparison of the peak lateral force coefficients for both flippers at varying AR. Simulation points are depicted as ∘ while the dashed lines represent the best fit curves.*

AR, the vortex appears to be diffused due to interactions between the main LEV and the tip. As AR increases, the spanwise-averaged LEV becomes more coherent and its circulation rises (for a given box size). However, this value starts to level off at higher AR, following the same trend as the thrust coefficient. It can also be seen that the circulation values in the back foil are significantly higher than that of the front foil, in accordance with the thrust results.

Similarly to the findings of section 3.1, values of $C_{Y,max}$ follow a saturating pattern with increasing flipper elongation (see figure 13b). Furthermore, by comparing peak $C_{Y,f}$ and $C_{Y,b}$, we notice relatively higher values for the latter. As mentioned previously, these loads are mostly associated to the added mass effects while circulatory forces are the major contributor in thrust generation. Therefore, we conclude that the combination of high AR and wake recapture, experienced by the aft flipper, leads not only to the stabilization but also the augmentation of both the circulatory and added mass forces.

3.3. Application concerns

Recent advancements in AUV technology have revealed an abundance of novel configurations, for a wide range of civilian and military applications (Budiyono, 2009; Weymouth et al., 2017). Undoubtedly, the effectiveness of these designs is heavily influenced by the specifications of the chosen propulsor. Having analysed the performance of such system, we now propose certain combinations that enable us to utilize the advantages of in-line flapping.

Previous chapters revealed a lack of coherence in the shed vortices of $AR \leq 4$. Another critical feature of low AR flippers, is the tendency of consecutive LEVs to travel further apart from the centerline, leading to more divergent streams (Dong et al., 2006; Shao et al., 2010). Indeed, figure 14 shows that the distance of successive vortices, normal to the hind foil's chord is larger at $AR = 2$, compared to $AR = 8$. This, combined with their aforementioned low cohesion, means that colliding with the back foil is both less probable and less critical for the latter's performance. Consequently, low AR´s permit a broader range of ϕ, leading to a more flexible service envelope. In other words, changes of the kinematic parameters (e.g. in St_A) that would result in a less optimal phasing, will not alter significantly the overall wake-flipper interactions.

High AR flippers, on the other hand, would be preferable for steady cruising, namely constant speed at undisturbed kinematic conditions. This is probably supported by natural evolution examples, as fossils of the long-distance swimming *plesiosauromorphs* indicate $AR \geq 8$ (O'Keefe, 2001). Having said that, tandem arrangements of $AR \sim [4-6]$ may be a prudent compromise between augmentation

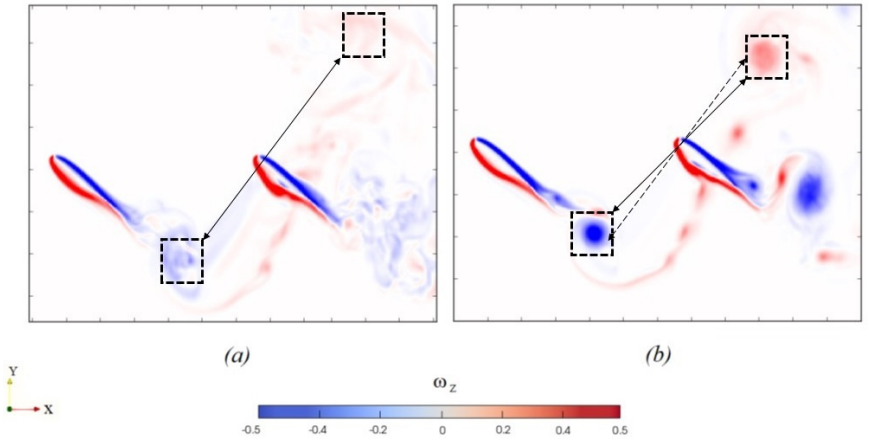

Figure 14. *Spanwise averaged vorticity of the tandem configuration at $t/T = 1$, for (a) $AR = 2$ and (b) $AR = 8$. Boxes of black dashed line mark the boundaries of consecutive shed vortices while the distance between them is highlighted by black arrows. Notice how this is reduced as we move to higher AR (solid vs dashed arrows).*

benefits and mechanical behaviour, since the relative thrust enhancement has reached a saturated state while the size is still small enough to withstand the large unsteady loads.

Finally, a set of mixed AR can be a further improvement in cases where LEV breakdown has not developed significantly by the time it reaches the hind foil (e.g. low $\mathcal{S}_C$ and average/high flipper slenderness). More specifically, we speculate that a shorter rear flipper ($\sim$ lower AR) would be able to avoid the disturbances of the front wingtip, functioning completely within the quasi-2D stream. In fact, this strategy can lead to an increase of $\tilde{C_{T,b}}$ by up to 8% in dragonfly-inspired concepts (Jurado et al., 2022) and it was likely utilized by certain plesiosaur species (O'Keefe, 2001).

4. Conclusions and future work

The propulsive characteristics of single and tandem flapping foils were examined numerically under a heave-to-pitch coupling motion, for seven flipper sets of $AR \sim [2-8]$ of rectangular flippers with elliptical tip at $Re_C = 8500$. Each set had the same AR and the test were conducted for the fixed combination $St_A = 0.4 - \mathcal{S}_C = 2$ at $\phi = 0^o$ which was found to optimise wake recapture in 2D.

Our analysis shows that flipper elongation has a positive impact on the phase-averaged thrust and peak lateral force of both single and tandem configurations at low AR´s but this effect weakens as we move towards higher AR. More specifically, an increasing AR benefits the wake recapture of the tandem configuration, which results in a slower convergence of the back flipper´s hydrodynamic forces. On the other hand the efficiency remains virtually unaffected due to the foils´ optimal kinematics and the thrust-targeting ϕ.

Physically, the behaviour of thrust is related to the enhanced strength and cohesion of the vortex pair shed at each cycle. In particular, snapshots of instantaneous vorticity show that 3D effects have a localized behaviour around the wing tip of the front foil which remains constant throughout the range of AR´s. This affects spanwise-averaged LEV circulation, which increases with elongation but eventually saturates, so that the growth of $\tilde{C_T}$ diminishes towards two dimensional concepts ($AR \sim \infty$). Low AR´s, however, lead to weaker LEVs which move away from the centerline and decay faster in the streamwise direction. This is vital for the hind flipper as a stronger incoming wake will induce higher acceleration of the surrounding flow while a wider, weaker vortex pair can enable a greater range of ϕ since weaving within the vortices becomes easier. Consequently, wake recapture leads to an augmented Γ for the LEV of the rear foil, combined with a higher sensitivity towards flipper slenderness. This

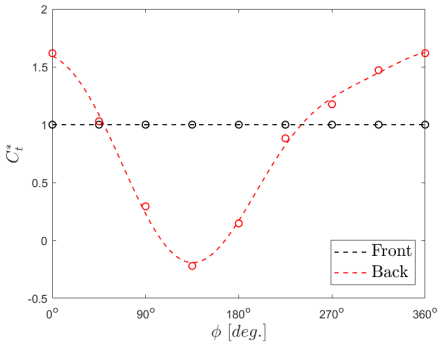

Figure 15. *Impact of ϕ on the two dimensional wake recapture, expressed via the relative thrust augmentation of the two foils. Here $C^*_{T,f} = 1$ since the front foil experiences no flow field changes, which coincides with $\tilde{C_{t,f}} \sim 0.675$. Simulation points are depicted as $\circ$ while the dashed lines represent the best fit curves.*

results in a comparatively sharper circulation increase and a slower convergence, following the pattern of $\tilde{C_T}$ results, probably due to the prevalence of circulatory forces in heave-dominant motions. As the peak lateral forces show a similar trend with AR, it is possible that the added mass-induced, force components are affected in an analogous manner.

This study provides evidence of the AR impact on wake recapture under kinematics commonly used in the natural world. In addition, our findings provide hints for the design of more versatile bio-inspired systems by revealing the hydrodynamic benefits and limitations of the single and tandem flipper arrangements. This is based on the singular effect of aspect ratio been addressed here for a simple spanwise geometry. However, natural systems can achieve a wide range of planforms for the same aspect ratio while it is possible to expand this design range through advanced engineering tools, used in modern industry. Therefore, we believe that the effects of planform shape can be further explored at a given aspect ratio that is optimized for a particular tandem foil concept.

APPENDIX

A. Phase optimisation

To set our reference test case in terms of maximum thrust augmentation, a preliminary study was conducted in 2D, evaluating the phasing ϕ of the tandem configuration for the chosen spacing, kinematic parameters and ambient conditions. Tandem foil simulations were performed, starting from $\phi = 0^o$ and progressing at increments of $\Delta\phi = 45^o$ until $\phi = 315^o$, while the single foil was found to produce $\tilde{C_{t,f}} \sim 0.675$. Figure 15 shows that the modification of the hind foil´s thrust due to interacting with the incoming wake, follows a cosine-like curve with respect to the phase lag, as shown in similar studies (Muscutt et al., 2017a). Clearly, optimal $C^*_{T,b}$ is found for $\phi = 0^o$ and therefore it is chosen for all the simulations presented in the current study.

B. Sensitivity analysis of the LEV circulation

In this study, circulation is calculated via the integration of vorticity over a rectangular cell (see figure 16a). As we focus on the LEV analysis, the size and location of this area should be optimized to enclose the exact size of the vortex while minimizing ambient interference. Therefore, after visually choosing an initial location, we gradually increase the area of integration until the overall circulation begins to drop (see figure 16b). Having finalized the size of the box, we re-evaluate its location by moving its center towards the y and x axis until a position of maximum circulation is identified. Due to the shape/size of

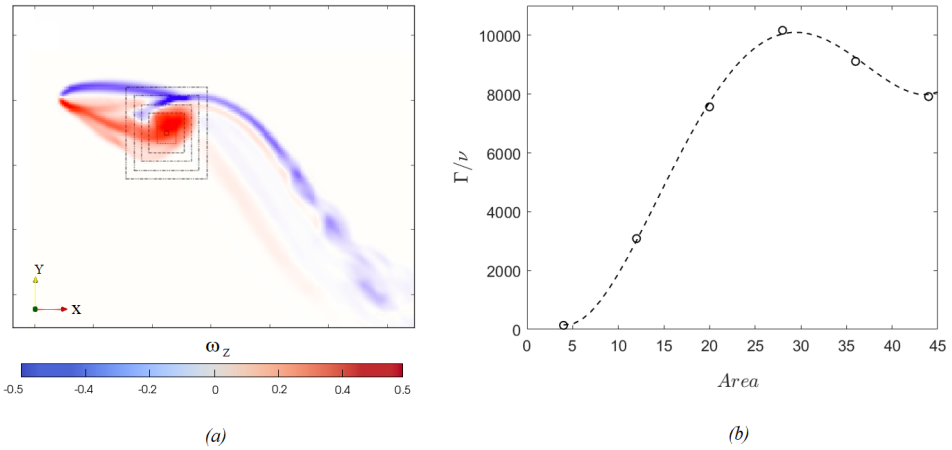

Figure 16. *Sensitivity analysis of the integration area, used to calculate the circulation of the front foil´s LEV. Here the vorticity is first spanwise averaged, at* $t/T = 0.25$ *as shown in (a) for* $AR = 2$*. Then it is integrated within boxes of increasing size until circulation values begin to drop (b).*

the LEV for various ARs, this procedure was conducted individually for all single and tandem test cases such that the "highest" circulation is obtained for each case.

Acknowledgements. We would like to thank A.N. Zurman-Nasution and M. Lauber for our fruitful discussions throughout the duration of this project. Furthermore, we would like to thank the IRIDIS High Performance Computing Facility, with its associated support services at the University of Southampton, for their aid towards the completion of our study.

Funding statement. This research was supported financially by the Office of Naval Research award N62909-18-1-2091 and the Engineering and Physical Sciences Research Council doctoral training award [1789955].

Declaration of interests. The authors declare no conflict of interest.

Author contributions. Conceptualization: N.S.L, G.W. and B.G. Investigation: N.S.L. Writing original draft: N.S.L. Writing review and editing: G.W. and B.G.

Data availability statement. All data supporting this study, including useful supplementary material, is openly available via the University of Southampton repository at (AVAILABLE UPON ACCEPTANCE).

Ethical standards. The research meets all ethical guidelines, including adherence to the legal requirements of the study country.

References

Adams, D. S. and Fish, F. E. (2019). Odontocete peduncle tendons for possible control of fluke orientation and flexibility. *Journal of morphology*, 280(9):1323–1331.

Akhtar, I., Mittal, R., Lauder, G. V., and Drucker, E. (2007). Hydrodynamics of a biologically inspired tandem flapping foil configuration. *Theoretical and Computational Fluid Dynamics*, 21(3):155–170.

Alexander, D. E. (1984). Unusual phase relationships between the forewings and hindwings in flying dragonflies. *Journal of Experimental Biology*, 109(1):379–383.

Arranz, G., Flores, O., and Garcia-Villalba, M. (2020). Three-dimensional effects on the aerodynamic performance of flapping wings in tandem configuration. *Journal of Fluids and Structures*, 94:102893.

Ayancik, F., Fish, F. E., and Moored, K. W. (2020). Three-dimensional scaling laws of cetacean propulsion characterize the hydrodynamic interplay of flukes' shape and kinematics. *Journal of the Royal Society Interface*, 17(163):20190655.

Azuma, A. (1992). Flight by beating. In *The Biokinetics of Flying and Swimming*, pages 77–154. Springer.

Boschitsch, B. M., Dewey, P. A., and Smits, A. J. (2014). Propulsive performance of unsteady tandem hydrofoils in an in-line configuration. *Physics of Fluids*, 26(5):051901.

Broering, T. M. and Lian, Y. (2015). Numerical study of tandem flapping wing aerodynamics in both two and three dimensions. *Computers & Fluids*, 115:124–139.

Broering, T. M. and Lian, Y.-S. (2012). The effect of phase angle and wing spacing on tandem flapping wings. *Acta Mechanica Sinica*, 28(6):1557–1571.

Budiyono, A. (2009). Advances in unmanned underwater vehicles technologies: Modeling, control and guidance perspectives.

Carpenter, K., Sanders, F., Reed, B., Reed, J., and Larson, P. (2010). Plesiosaur swimming as interpreted from skeletal analysis and experimental results. *Transactions of the Kansas Academy of Science*, 113(1/2):1–34.

Cimarelli, A., Franciolini, M., and Crivellini, A. (2021). On the kinematics and dynamics parameters governing the flow in oscillating foils. *Journal of Fluids and Structures*, 101:103220.

Combes, S. and Daniel, T. (2001). Shape, flapping and flexion: wing and fin design for forward flight. *Journal of Experimental Biology*, 204(12):2073–2085.

Dagenais, P. and Aegerter, C. M. (2020). How shape and flapping rate affect the distribution of fluid forces on flexible hydrofoils. *Journal of Fluid Mechanics*, 901.

Dewey, P. A., Boschitsch, B. M., Moored, K. W., Stone, H. A., and Smits, A. J. (2013). Scaling laws for the thrust production of flexible pitching panels. *Journal of Fluid Mechanics*, 732:29.

Domenici, P. (2010). *Fish locomotion: an eco-ethological perspective*. CRC Press.

Dong, H., Mittal, R., and Najjar, F. (2006). Wake topology and hydrodynamic performance of low-aspect-ratio flapping foils. *Journal of Fluid Mechanics*, 566:309.

Ellington, C. P. (1984). The aerodynamics of hovering insect flight. ii. morphological parameters. *Philosophical Transactions of the Royal Society of London. B, Biological Sciences*, 305(1122):17–40.

Epps, B. P., Muscutt, L. E., Roesler, B. T., Weymouth, G. D., and Ganapathisubramani, B. (2017). On the interfoil spacing and phase lag of tandem flapping foil propulsors. *Journal of Ship Production and Design*, 33(04):276–282.

Fernandez-Feria, R. and Alaminos-Quesada, J. (2021). Analytical results for the propulsion performance of a flexible foil with prescribed pitching and heaving motions and passive small deflection. *Journal of Fluid Mechanics*, 910.

Fish, F. E. and Rohr, J. (1999). Review of dolphin hydrodynamics and swimming performance.

Flammang, B. E. and Lauder, G. V. (2009). Caudal fin shape modulation and control during acceleration, braking and backing maneuvers in bluegill sunfish, lepomis macrochirus. *Journal of Experimental Biology*, 212(2):277–286.

Floryan, D., Van Buren, T., Rowley, C. W., and Smits, A. J. (2017). Scaling the propulsive performance of heaving and pitching foils. *Journal of Fluid Mechanics*, 822:386–397.

Gough, W. T., Fish, F. E., Wainwright, D. K., and Bart-Smith, H. (2018). Morphology of the core fibrous layer of the cetacean tail fluke. *Journal of morphology*, 279(6):757–765.

Green, M. A. and Smits, A. J. (2008). Effects of three-dimensionality on thrust production by a pitching panel. *Journal of fluid mechanics*, 615:211–220.

Guglielmini, L. and Blondeaux, P. (2004). Propulsive efficiency of oscillating foils. *European Journal of Mechanics-B/Fluids*, 23(2):255–278.

Hammer, P. R., Garmann, D. J., and Visbal, M. (2021). Aspect ratio effect on finite wing dynamic stall. In *AIAA Scitech 2021 Forum*, page 1089.

Han, P., Wang, J., Fish, F. E., and Dong, H. (2020). Kinematics and hydrodynamics of a dolphin in forward swimming. In *AIAA AVIATION 2020 FORUM*, page 3015.

Hawthorne, M., McMenamin, M., and De la Salle, P. (2019). How plesiosaurs swam: New insights into their underwater flight using "ava", a virtual pliosaur.

Hendrickson, K., Weymouth, G. D., Yu, X., and Yue, D. K.-P. (2019). Wake behind a three-dimensional dry transom stern. part 1. flow structure and large-scale air entrainment. *Journal of Fluid Mechanics*, 875:854–883.

Joshi, V. and Mysa, R. C. (2021). Mechanism of wake-induced flow dynamics in tandem flapping foils: Effect of the chord and gap ratios on propulsion. *Physics of Fluids*, 33(8):087104.

Jurado, R., Arranz, G., Flores, O., and García-Villalba, M. (2022). Numerical simulation of flow over flapping wings in tandem: Wingspan effects. *Physics of Fluids*, 34(1):017114.

Karbasian, H. R. and Esfahani, J. (2017). Enhancement of propulsive performance of flapping foil by fish-like motion pattern. *Computers & Fluids*, 156:305–316.

Khalid, M. S. U., Wang, J., Akhtar, I., Dong, H., Liu, M., and Hemmati, A. (2021). Why do anguilliform swimmers perform undulation with wavelengths shorter than their bodylengths? *Physics of Fluids*, 33(3):031911.

Kim, D., Hussain, F., and Gharib, M. (2013). Vortex dynamics of clapping plates. *Journal of Fluid Mechanics*, 714:5–23.

King, J. T., Kumar, R., and Green, M. A. (2018). Experimental observations of the three-dimensional wake structures and dynamics generated by a rigid, bioinspired pitching panel. *Physical Review Fluids*, 3(3):034701.

Koochesfahani, M. (1989). Vortical patterns in the wake of an oscillating airfoil. *AIAA journal*, 27(9):1200–1205.

Lagopoulos, N., Weymouth, G., and Ganapathisubramani, B. (2020). Deflected wake interaction of tandem flapping foils. *Journal of Fluid Mechanics*, 903.

Lagopoulos, N. S., Weymouth, G. D., and Ganapathisubramani, B. (2019). Universal scaling law for drag-to-thrust wake transition in flapping foils. *Journal of Fluid Mechanics*, 872.

Lauber, M., Weymouth, G. D., and Limbert, G. (2022). Immersed boundary simulations of flows driven by moving thin membranes. *Journal of Computational Physics*, 457:111076.

Lee, J., Park, Y.-J., Cho, K.-J., Kim, D., and Kim, H.-Y. (2017). Hydrodynamic advantages of a low aspect-ratio flapping foil. *Journal of Fluids and Structures*, 71:70–77.

Leonard, B. P. (1979). A stable and accurate convective modelling procedure based on quadratic upstream interpolation. *Computer methods in applied mechanics and engineering*, 19(1):59–98.

Li, Y., Pan, D., Zhao, Q., Ma, Z., and Wang, X. (2018). Hydrodynamic performance of an autonomous underwater glider with a pair of bioinspired hydro wings–a numerical investigation. *Ocean Engineering*, 163:51–57.

Licht, S., Polidoro, V., Flores, M., Hover, F. S., and Triantafyllou, M. S. (2004). Design and projected performance of a flapping foil auv. *IEEE Journal of oceanic engineering*, 29(3):786–794.

Long, J. H., Schumacher, J., Livingston, N., and Kemp, M. (2006). Four flippers or two? tetrapodal swimming with an aquatic robot. *Bioinspiration and Biomimetics*, 1(1):20.

Maertens, A. and Weymouth, G. (2015). Accurate cartesian-grid simulations of near-body flows at intermediate reynolds numbers. *Computer Methods in Applied Mechanics and Engineering*, 283:106 – 129.

Mittal, R. (2004). Computational modeling in biohydrodynamics: Trends, challenges, and recent advances. *IEEE Journal of Oceanic Engineering*, 29(3):595–604.

Muscutt, L. E., Dyke, G., Weymouth, G. D., Naish, D., Palmer, C., and Ganapathisubramani, B. (2017a). The four-flipper swimming method of plesiosaurs enabled efficient and effective locomotion. *Proceedings of the Royal Society B: Biological Sciences*, 284(1861):20170951.

Muscutt, L. E., Weymouth, G. D., and Ganapathisubramani, B. (2017b). Performance augmentation mechanism of in-line tandem flapping foils. *Journal of Fluid Mechanics*, 827:484–505.

O'Keefe, F. R. (2001). Ecomorphology of plesiosaur flipper geometry. *Journal of Evolutionary Biology*, 14(6):987–991.

O'Keefe, F. R. and Carrano, M. T. (2005). Correlated trends in the evolution of the plesiosaur locomotor system. *Paleobiology*, 31(4):656–675.

Ol, M. V., Bernal, L., Kang, C.-K., and Shyy, W. (2010). Shallow and deep dynamic stall for flapping low reynolds number airfoils. In *Animal Locomotion*, pages 321–339. Springer.

Pedro, G., Suleman, A., and Djilali, N. (2003). A numerical study of the propulsive efficiency of a flapping hydrofoil. *International journal for numerical methods in fluids*, 42(5):493–526.

Platzer, M. and Jones, K. (2008). Flapping wing aerodynamics-progress and challenges. In *44th AIAA Aerospace Sciences Meeting and Exhibit*, page 500.

Polet, D., Rival, D., and Weymouth, G. (2015). Unsteady dynamics of rapid perching manoeuvres. *Journal of Fluid Mechanics*, 767:323–341.

Robinson, J. A. and JA, R. (1975). The locomotion of plesiosaurs.

Shao, X.-m., Pan, D.-y., Deng, J., and Yu, Z.-s. (2010). Numerical studies on the propulsion and wake structures of finite-span flapping wings with different aspect ratios. *Journal of Hydrodynamics*, 22(2):147–154.

Shi, G., Xiao, Q., and Zhu, Q. (2020). Effects of time-varying flexibility on the propulsion performance of a flapping foil. *Physics of Fluids*, 32(12):121904.

Thomas, A. L. R., Taylor, G. K., Srygley, R. B., Nudds, R. L., and Bomphrey, R. J. (2004). Dragonfly flight: free-flight and tethered flow visualizations reveal a diverse array of unsteady lift-generating mechanisms, controlled primarily via angle of attack. *Journal of Experimental Biology*, 207(24):4299–4323.

Triantafyllou, G., Triantafyllou, M., and Grosenbaugh, M. (1993). Optimal thrust development in oscillating foils with application to fish propulsion. *Journal of Fluids and Structures*, 7(2):205–224.

Triantafyllou, M., Triantafyllou, G., and Gopalkrishnan, R. (1991). Wake mechanics for thrust generation in oscillating foils. *Physics of Fluids A: Fluid Dynamics*, 3(12):2835—-2837.

Usherwood, J. R. and Ellington, C. P. (2002). The aerodynamics of revolving wings ii. propeller force coefficients from mayfly to quail. *Journal of Experimental Biology*, 205(11):1565–1576.

Usherwood, J. R. and Lehmann, F.-O. (2008). Phasing of dragonfly wings can improve aerodynamic efficiency by removing swirl. *Journal of The Royal Society Interface*, 5(28):1303–1307.

Van Buren, T., Floryan, D., and Smits, A. J. (2019). Scaling and performance of simultaneously heaving and pitching foils. *AIAA Journal*, 57(9):3666–3677.

Walker, J. A. and Westneat, M. W. (2002). Performance limits of labriform propulsion and correlates with fin shape and motion. *Journal of Experimental Biology*, 205(2):177–187.

Weymouth, G., Devereux, K., Copsey, N., Muscutt, L., Downes, J., and Ganapathisubramani, B. (2017). Hydrodynamics of an under-actuated plesiosaur-inspired robot. *APS*, pages F9–003.

Weymouth, G. and Yue, D. (2011). Boundary data immersion method for cartesian-grid simulations of fluid-body interaction problems. *Journal of Computational Physics*, 230(16):6233 – 6247.

Weymouth, G. D. (2016). Biologically inspired force enhancement for maritime propulsion and maneuvering. *arXiv preprint arXiv:1609.06559*.

Woodward, B. L., Winn, J. P., and Fish, F. E. (2006). Morphological specializations of baleen whales associated with hydrodynamic performance and ecological niche. *Journal of Morphology*, 267(11):1284–1294.

Xu, G., Duan, W., and Xu, W. (2017). The propulsion of two flapping foils with tandem configuration and vortex interactions. *Physics of Fluids*, 29(9):097102.

Yuh, J. (2000). Design and control of autonomous underwater robots: A survey. *Autonomous Robots*, 8(1):7–24.

Zhong, Q., Han, T., Moored, K. W., and Quinn, D. B. (2021). Aspect ratio affects the equilibrium altitude of near-ground swimmers. *Journal of Fluid Mechanics*, 917.

Zurman-Nasution, A., Ganapathisubramani, B., and Weymouth, G. (2020). Influence of three-dimensionality on propulsive flapping. *Journal of Fluid Mechanics*, 886.

Zurman-Nasution, A. N., Ganapathisubramani, B., and Weymouth, G. D. (2021a). Effects of aspect ratio on rolling and twisting foils. *Physical Review Fluids*, 6(1):013101.

Zurman-Nasution, A. N., Ganapathisubramani, B., and Weymouth, G. D. (2021b). Fin sweep angle does not determine flapping propulsive performance. *Journal of the Royal Society*, 18.

Cite this article: N. S. Lagopoulos, G. D. Weymouth and B. Ganapathisubramani (2021). Effect of aspect ratio on the propulsive performance of tandem flapping foils. *Flow*, *This draft was prepared using the LaTeX style file belonging to FLOW: Applications of Fluid Mechanics*, E1. doi: